https://doi.org/10.65091/icicset.v2i1.33

Change Detection in Land Surface Temperature After Construction of Pokhara International Airport using Remote Sensing

Narayan Puri
Department of Civil Engineering
Nepal College of Information Technology
Pokhara University
Lalitpur, Nepal
narayan.puri@ncit.edu.np

Shree Krishna Yadav
Department of Computer Engineering
Nepal College of Information Technology
Pokhara University
Lalitpur, Nepal
shreekrishna@ncit.edu.np

Ashim Khadka*
Department of Computer Engineering
Nepal College of Information Technology
Pokhara University
Lalitpur, Nepal
ashim.khadka@ncit.edu.np

*Corresponding author

***Abstract*—This study quantifies the thermal environmental impact of Pokhara International Airport in Nepal by analyzing land surface temperature (LST) trends before and after its construction. Using the Google Earth Engine (GEE) platform, TerraClimate (1987-2025) and MODIS datasets are processed to perform a spatiotemporal analysis across two distinct periods from pre-construction (i.e., 1987-2017) and post-construction (i.e., 2018-2025) of Pokhara International Airport. The derived LST trends is validated through zonal analysis of urban heat island (UHI) intensity using urban (500 m, 1 km) and rural (2-4 km) buffers and correlated with a time-series analysis of the Normalized Difference Vegetation Index (NDVI). The results indicate a pronounced acceleration in warming following the airport's construction, with the LST trend rising from $0.44^{\circ}C$/decade in the pre-construction period to $2.53^{\circ}C$/decade afterwards. Statistical validation via the Mann–Kendall test and Sen's slope estimator confirmed a significant increasing trend ($p < 0.001$). This warming is coupled with a strengthening of the UHI effect, where the mean urban–rural LST difference increased from $0.5^{\circ}C$ to $1.34^{\circ}C$, and a sustained decline in NDVI, signifying vegetation loss. The findings demonstrate that major infrastructure projects can rapidly alter local microclimates, exacerbating surface warming and UHI effects.**

***Index Terms*—Land Surface Temperature, Urban Heat Island, Remote Sensing, Climate Change, Infrastructure Impact**

I. Introduction

One of the most pressing challenges of the 21st century is climate change, with land surface temperature (LST) serving as a critical indicator of environmental change. Land surface temperature (LST) serves as a primary indicator of climate change and environmental health, directly influencing ecological processes, urban microclimates, and human well-being. Urban expansion and large-scale infrastructure development are among the primary drivers of land cover transformation and local climate modification worldwide [1]. Large infrastructure, such as airports, is recognized as a major contributor to localized surface warming due to extensive impervious surfaces, vegetation clearance, and high-energy activities. In developing countries, rapid infrastructure growth often occurs with limited consideration of environmental and climatic impacts, exacerbating urban heat island (UHI) effects [2], [3].

Pokhara, Nepal-a metropolitan and tourist capital city in the Himalayan foothills-has experienced accelerated urban expansion in recent decades, accompanied by substantial changes in land use and land cover. The construction of Pokhara International Airport, operationalized in 2022, represents one of the most substantial infrastructure interventions in the region. While such projects are critical for economic growth and enhance regional connectivity, their environmental implications—particularly on land surface temperature–remain insufficiently documented [4]. Previous study conducted in Pokhara and Bharatpur metropolitan cities [5], a multi-fold increase in built-up areas along with a plunge in agricultural lands was found from 1990 to 2018, which may result in increased LST and corresponding UHI effect [6]. However, a targeted investigation into the thermal impact of a singular, large-scale infrastructure project like an airport remains lacking.

Recent advancements in cloud computing platforms, particularly Google Earth Engine (GEE), have revolutionized the capacity to conduct reproducible, large-scale environmental analyses [7]. Remote sensing and geospatial platforms such as GEE provide efficient access and processing of long-term remote sensing data enabling robust trend analysis and change detection. TerraClimate is a high-resolution global climate dataset, enables consistent assessment of temperature variability at monthly scales [8], [9]. When integrated with vegetation indicators such as the Normalized Difference Vegetation Index (NDVI), allow for a holistic evaluation of land cover and its thermal behavior [10].

This study aims to quantify the change in land surface temperature before and after the construction of Pokhara International Airport and evaluate associated changes in vegetation cover and UHI intensity. Specifically, the research objectives are to:

1 Analyze long-term LST, UHI and NDVI temporal trends before and after the construction of Pokhara International Airport

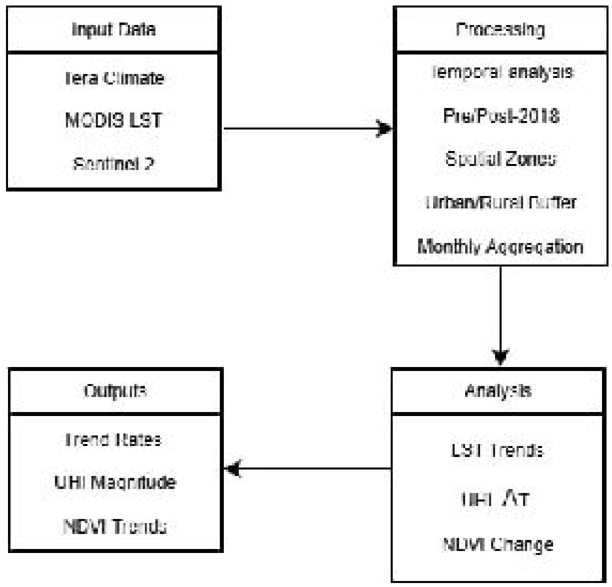

Fig. 1: Proposed Workflow of the study

2 Evaluate spatial temperature differences between urban (airport) and rural zones
3 Quantify the thermal impact of airport-induced land cover changes

The findings of this study will offer evidence-based insights into the local climatic impacts of major infrastructure, supporting informed urban and environmental planning in rapidly developing regions such as Nepal.

The rest of the paper is organized as follows: Section II includes the details of the entire process and the model used. Section III discusses the detailed results. Finally, a conclusion is in section IV.

II. Materials and Methods

The overall proposed methodological framework of the study is shown in Fig. 1, which integrates data acquisition, preprocessing, analysis, and validation.

A. Study Area

The analysis focuses on a geographical region centered at Pokhara International Airport [84.0148°E, 28.1838°N], representing a concrete paved urban land cover as shown in fig. 2. The study area encompasses a 1000-meter radius circular region around the selected point for localized temperature analysis. After the construction of the airport, the urbanization expansion has increased rapidly, which also influences the land surface temperature. Pokhara valley, where the airport is located, lies geographically between 83.9750° to 84.0342°E and 28.1667° to 28.2667°N, at an elevation range from 827 to 1,740 meters above Mean Sea Level (MSL). Summer temperatures average 30°C to 32°C, while winter temperatures range from 6°C to 8°C [11]. The analysis specifically focuses on three concentric zones surrounding of the airport: (1) an urban core zone defined by a 500 m radius buffer representing the immediate airport infrastructure, (2) an urban influence zone with a 1 km radius buffer encompassing the airport and its immediate vicinity, and (3) a rural reference zone comprising a 2-4 km concentric ring representing less-developed peri-urban areas. This zonal approach enables comparative analysis of localized thermal impacts against background conditions.

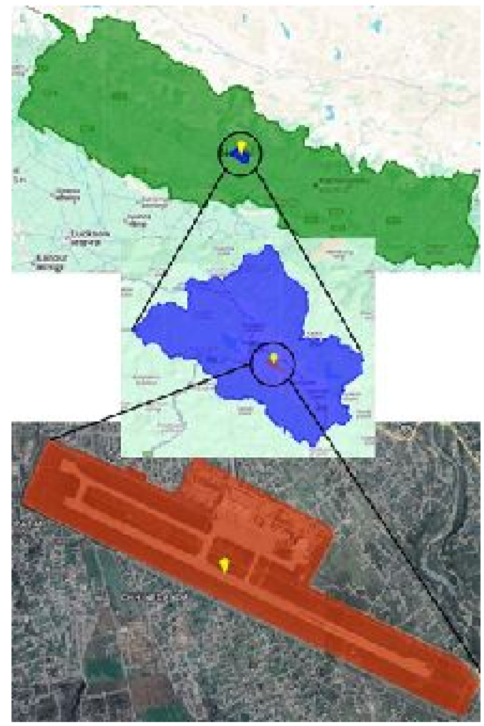

Fig. 2: Geolocations map of Pokhara International Airport as the study Area

B. Data Sources and Preprocessing

This study utilized multi-source remote sensing and climate data processed within the GEE cloud platform (Table I). GEE provides computational infrastructure for large-scale geospatial analysis without requiring local data storage or high-performance computing resources [9].

TABLE I: Summary of datasets used in the study.

Dataset	**Spatial Resolution**	**Temporal Resolution**	**Time Period**
TerraClimate [12]	∼4 km	Monthly	1958–Present
MODIS MOD11A1 V6.1 [13]	1 km	Daily	2000–2025
Sentinel-2 MSI [14]	10–20 m	5 days	2015–2025

1) Climate Data (TerraClimate): The TerraClimate dataset provides globally gridded monthly climate data derived through spatial interpolation of station observations and climatically aided extrapolation. Monthly minimum (t_{min}) and maximum (t_{max}) air temperature layers were accessed via GEE. The monthly mean temperature, calculated as $(t_{min} + t_{max})/2$, served as a proxy for land surface temperature for long-term (1987–2025) trend analysis, given its high temporal consistency and suitability for climate trend studies [8], [12].

2) Thermal Remote Sensing Data (MODIS): The MODIS Terra Land Surface Temperature and Emissivity product (MOD11A1 V6.1) provides daily LST retrievals under clear-sky conditions at 1 km spatial resolution [13]. Daily daytime LST data were filtered for quality (using QC_Day layer ≤ 1), masked for clouds, and aggregated to monthly means. This dataset was used exclusively for the higher-resolution spatial analysis of UHI effects from 2001 onward [4].

3) Optical Satellite Imagery (Sentinel-2): Sentinel-2 MultiSpectral Instrument (MSI) Level-2A surface reflectance data were used to compute the Normalized Difference Vegetation Index (NDVI) [14]. Images were filtered for cloud cover ($< 20\%$) using the scene classification layer (SCL). NDVI was calculated per-pixel based on Band 8 (NIR) and Band 4 (Red).

4) Ancillary Data: A polygon delineating the Pokhara International Airport boundary was digitized from high-resolution basemaps in ArcGIS and imported into GEE for spatial extractions.

C. Temporal Framework

The analysis period was divided into two distinct phases based on the construction timeline of Pokhara International Airport:

1) Pre-construction Period (1987-2017): 31-year baseline period before major airport construction activities commenced (i.e., pre-2018).

2) Post-construction Period (2018-2025): 8-year period encompassing airport construction from 2018 to 2021 and the operational phase from 2022 to 2025.

This temporal partitioning enables direct comparison of thermal conditions before and after the infrastructure intervention.

D. Analytical Methods

1) LST Trend Analysis: Monthly mean temperature was extracted from TerraClimate for the urban buffer zone and aggregated to annual means. The trend magnitude was expressed as °C per decade to facilitate comparison with global climate change metrics [3].

2) NDVI Analysis: NDVI was computed for all cloud-free Sentinel-2 imagery to generate time series that reflect vegetation changes across periods of imagery using:

$$NDVI = \frac{\rho_{NIR} - \rho_{Red}}{\rho_{NIR} + \rho_{Red}} \tag{1}$$

where ρ_{NIR} is reflectance in the near-infrared band (Band 8), and ρ_{Red} is reflectance in the red band (Band 4). Seasonal median NDVI composites were generated for the monsoon period (July–September) each year to minimize seasonal variability and focus on peak vegetation conditions [15], [16].

(a) Urban buffer with 500 radius

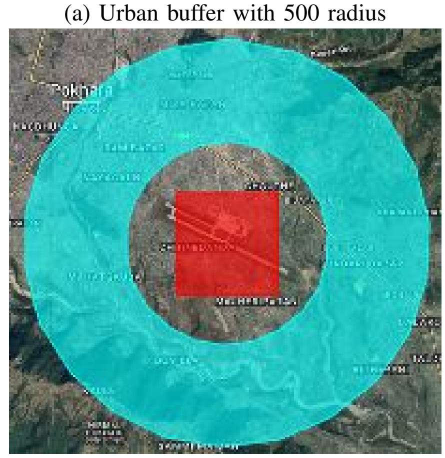

(b) Urban buffer with 1 km radius

Fig. 3: Buffer zone having urban and rural radius

3) UHI Quantification: UHI intensity was quantified as the temperature difference between urban and rural zones is given by

$$\Delta T = \overline{LST}_{urban} - \overline{LST}_{rural} \tag{2}$$

where $\overline{LST}_{urban}$ is the mean LST within urban buffers (500 m or 1 km radius) and $\overline{LST}_{rural}$ is the mean LST within the rural reference zone (2–4 km ring) as shown in 3. Monthly mean LST values from MODIS were extracted for each zone, and annual mean ΔT was computed for both temporal periods.

4) Statistical Trend Validation: Mann-Kendall (MK) Test is non-parametric test used to detect monotonic trends in time series data without assuming normal distribution [14]. The test statistic S is calculated as

$$S = \sum_{i=1}^{n-1} \sum_{j=i+1}^{n} sgn(x_j - x_i) \tag{3}$$

where x_i and x_j are sequential data values, n is the dataset length, and sgn is the sign function.

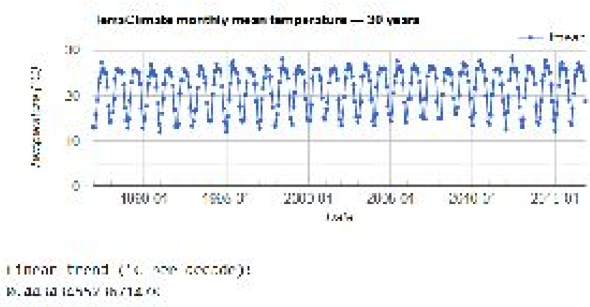

Fig. 4: Temporal variation of monthly mean LST before the construction of the airport

Fig. 5: Temporal variation of monthly mean LST before the construction of the airport

Sen's Slope Estimator is non-parametric method to quantify trend magnitude. The slope β is calculated as the median of all pairwise slopes using

$$\beta = \text{median}\left(\frac{x_j - x_i}{j - i}\right) \quad \text{for all } i < j \tag{4}$$

where positive β indicates increasing trends and negative β indicates decreasing trends.

III. Results and Discussion

A. Temporal Temperature Trends

Fig. 4 illustrates the time-series analysis of the land surface temperature trends for the 30-year span before the construction of the Pokhara International Airport. The pre-construction period (1988–2017) exhibited a linear warming trend of $0.44°C$ per decade, consistent with regional climate patterns. In contrast, the post-construction period (2018–2025) showed a 5.7-fold increase in warming rate to $2.53°C$ per decade as shown in fig. 5. The temperature near Pokhara International Airport has increased at an alarming rate after the construction of the airport. The magnitude of change suggests that infrastructure-induced warming can outpace background climate change in localized contexts. The magnitude of the change suggests that, under certain localized conditions, infrastructure-induced warming may exceed background climate change. Statistical validation confirmed the significance of these trends. The Mann-Kendall test yielded a Z-statistic of 3.675 with a p-value of 0.0002, indicating a highly significant increasing trend ($p < 0.001$). Sen's slope estimator quantified the overall warming rate at $0.0369°C$/year ($0.37°C$/decade), with the trend remaining significant after correcting for serial autocorrelation as shown in Table II.

TABLE II: Statistical significance test results using Mann-Kendall and Sen's slope

MANN–KENDALL TEST RESULTS	
Trend:	increasing
Z-statistic:	3.675
P-value:	0.0002
Kendall Tau:	0.476
SEN'S SLOPE RESULTS	
Slope:	$0.0369°C$/year
Intercept:	20.800

TABLE III: UHI effect on urban buffer zone with 500m and 1 km radius and rural reference zone (2–4 km ring)

UHI Effect for 500 m Buffer Zone			
Parameter	Pre-construction (2001–2017)	Post-construction (2018–2025)	Change
Mean Urban LST	$26.099°C$	$26.484°C$	$+0.385°C$
Mean Rural LST	$25.598°C$	$25.143°C$	$-0.455°C$
UHI Intensity (ΔT)	$0.501°C$	$1.341°C$	+168%
UHI Effect for 1 km Buffer Zone			
Parameter	Pre-construction (2000–2017)	Post-construction (2018–2025)	Change
Mean Urban LST	$26.157°C$	$26.343°C$	$+0.186°C$
Mean Rural LST	$25.598°C$	$25.143°C$	$-0.455°C$
UHI Intensity (ΔT)	$0.559°C$	$1.200°C$	+114%

The urban heat island analysis demonstrated significant intensification following airport construction across both buffer zones as shown in Table III. For the 500 m urban buffer, UHI intensity (ΔT) increased from $0.50°C$ during 2001–2017 to $1.34°C$ during 2018–2025—a 168% increase. Similarly, the 1 km buffer showed UHI intensification from $0.56°C$ to$1.20°C$ (114% increase). The stronger UHI effect in the 500 m buffer ($1.34°C$) compared to the 1 km buffer ($1.20°C$) suggests that thermal impacts are most pronounced immediately adjacent to the airport infrastructure. The concurrent cooling in rural zones ($-0.455°C$) may reflect background climate variability and an increase in afforestation, but the consistent urban-rural temperature gradient increase confirms UHI strengthening. This rate of warming ($\sim 0.37°C$ per decade) is notably higher than the global average surface warming rate observed since the pre-industrial era (approx. $0.08°C$/decade since 1880) and even the more recent rapid warming (approx. $0.18°C$/decade over the last 40 years).

B. NDVI Variation

Fig. 6 shows the NDVI time-series analysis which revealed substantial vegetation decline following airport construction. Pre-construction monsoon season (July–September) NDVI values averaged +0.60, indicating healthy vegetation cover. Post-construction values rarely exceeded +0.40 during the same period, representing an approximate 33% reduction in vegetation

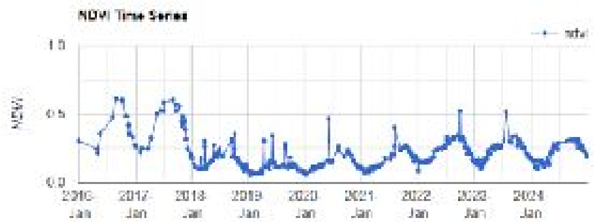

Fig. 6: NDVI time-series analysis indicating vegetation change associated with airport development

vigor. The NDVI time-series showed a pronounced downward trend post-2018, with the most significant declines occurring during peak construction years (2019–2021). This reduction was particularly evident during monsoon months when vegetation typically reaches peak greenness in the region. This indicates there is significant vegetative cover loss after the construction of the airport. This suggests that vegetation loss represents a permanent land cover transformation rather than seasonal variation.

The observed increasing trends in LST and UHI and decreasing trends in NDVI align with findings from similar airport-related urban studies [2], [5], [17]. Large impervious surfaces, reduced evapotranspiration, and altered surface albedo contribute significantly to surface warming. The $1.3°C$ urban–rural temperature differential within just 4 km radius apart indicates a strong localized UHI effect, which may exacerbate thermal discomfort, increase cooling energy demand, and elevate public health risks during heatwaves.

In Pokhara's context, the thermal impact is further influenced by valley topography and limited air circulation. The convergence of three independent lines of evidence—accelerated LST warming, intensified UHI effects, and substantial vegetation decline—provides robust confirmation of the Pokhara International Airport's thermal environmental impact.

The findings emphasize the need for integrating green infrastructure, reflective materials, and vegetation buffers in airport and urban planning. Specifically for Pokhara, climate-responsive design strategies should include high-albedo materials for paved surfaces, strategic vegetation buffers, and consideration of natural ventilation corridors in the valley setting.

IV. Conclusion

This study demonstrates that the construction of Pokhara International Airport has significantly altered local thermal conditions, resulting in accelerated land surface temperature increase, intensified urban heat island effects, and reduced vegetation cover. LST trends increased 5.7-fold from $0.44°C/$decade pre-construction to $2.53°C/$decade post-construction. Urban heat island effects strengthened by 114–168% across buffer zones, with temperature differentials reaching $1.34°C$. NDVI declined by approximately 33% during monsoon months, confirming extensive vegetation clearance. The application of TerraClimate data and GEE proved effective for long-term spatiotemporal climate assessment, providing a reproducible framework for similar investigations. The findings provide critical evidence for policymakers and planners to incorporate climate-sensitive design strategies in rapidly urbanizing regions. This study relies on moderate-resolution climate data ($\sim$ 4 km for TerraClimate, 1 km for MODIS), which may not capture micro-scale temperature variations within the airport complex. The use of TerraClimate air temperature as a proxy for land surface temperature, while suitable for trend analysis, may not fully represent surface thermal conditions for different land cover types.

References

[1] H. Piri Sahragard and P. Karami, "Spatiotemporal analysis of seasonal trends in land surface temperature within the distribution range of moringa peregrina (forssk.) in southern and southeastern iran," *PLOS ONE*, vol. 19, pp. 1–21, 07 2024. [Online]. Available: https://doi.org/10.1371/journal.pone.0306642

[2] A. Galodha and S. K. Gupta, "Land surface temperature as an indicator of urban heat island effect: A google earth engine based web-app," *The International Archives of the Photogrammetry, Remote Sensing and Spatial Information Sciences*, vol. XLIV-M-3-2021, pp. 57–62, 2021. [Online]. Available: https://isprs-archives.copernicus.org/articles/XLIV-M-3-2021/57/2021/

[3] R. Vohra, A. Kumar, R. Jain, and D. J. Hemanth, "Analysis and prediction of land surface temperature with increasing urbanisation using satellite imagery," *Heliyon*, vol. 10, no. 22, 2024.

[4] W. Zhao, J. He, Y. Wu, D. Xiong, F. Wen, and A. Li, "An analysis of land surface temperature trends in the central himalayan region based on modis products," *Remote Sensing*, vol. 11, no. 8, p. 900, 2019.

[5] R. Rai, Z. Yili, B. Paudel, N. R. Khanal, and B. K. Acharya, "Satellite image-based monitoring of urban land use change and assessing the driving factors in pokhara and bharatpur metropolitan cities, gandaki basin, nepal," *Journal of Resources and Ecology*, vol. 11, no. 1, pp. 87–99, 2020.

[6] P. Devkota, S. Dhakal, S. Shrestha, and U. B. Shrestha, "Land use land cover changes in the major cities of nepal from 1990 to 2020," *Environmental and Sustainability Indicators*, vol. 17, p. 100227, 2023.

[7] K. Onačillová, M. Gallay, D. Paluba, A. Péliová, O. Tokarčík, and D. Laubertová, "Combining landsat 8 and sentinel-2 data in google earth engine to derive higher resolution land surface temperature maps in urban environment," *Remote Sensing*, vol. 14, no. 16, p. 4076, 2022.

[8] J. T. Abatzoglou, S. Z. Dobrowski, S. A. Parks, and K. C. Hegewisch, "Terraclimate, a high-resolution global dataset of monthly climate and climatic water balance from 1958–2015," *Scientific data*, vol. 5, no. 1, pp. 1–12, 2018.

[9] T. Melese, G. Assefa, B. Terefe, T. Belay, G. Bayable, and A. Senamew, "Machine learning-based drought prediction using Palmer Drought Severity Index and TerraClimate data in Ethiopia," *PLoS One*, vol. 20, no. 6, p. e0326174, 2025.

[10] M. Mohammadnezhad, K. Davary, P. Shirazi, M. J. Rezvanpour, and S. M. Hasheminia, "A novel hybrid model for actual evapotranspiration estimation in data-scarce arid regions: Integrating modified Budyko and machine learning models using deep learning," *Science of The Total Environment*, vol. 1001, p. 180438, 2025.

[11] U. Jamarkattel, B. R. Lamichhane, S. Gautam, N. KC, B. Sherchan, and T. Horanont, "Analyzing Urban Heat Islands in Pokhara Metropolitan City-Nepal through Remote Sensing Techniques," *Remote Sensing Applications: Society and Environment*, vol. 37, p. 101479, 2025.

[12] M. M. Alemu, B. F. Zaitchick, T. Enku, A. W. Worqlul, E. A. Yimer, and A. van Griensven, "Evaluating hydroclimate dynamics: trend analysis and change detection for enhanced drought monitoring in the upper Blue Nile basin," *Journal of Water and Climate Change*, vol. 16, no. 8, pp. 2519–2537, 2025.

[13] Z. Wan, S. Hook, and G. Hulley, "MYD11A1 MODIS/aqua land surface temperature/emissivity daily L3 global 1km SIN grid V006," *NASA EOSDIS Land Processes Distributed Active Archive Center (DAAC) data set*, pp. MYD11A1–006, 2015.

[14] T. Semeraro, J. Titocci, L. Liberatore, F. Monti, F. De Leo, G. Ingrosso, M. Shokri, and A. Basset, “Analytical Workflow for Tracking Aquatic Biomass Responses to Sea Surface Temperature Changes,” *Environments*, vol. 12, no. 7, p. 210, 2025.
[15] A. Li, S. Yin, N. Li, and C. Shi, “Comprehensive Analysis of the Driving Forces Behind NDVI Variability in China Under Climate Change Conditions and Future Scenario Projections,” *Atmosphere*, vol. 16, no. 6, p. 738, 2025.
[16] E. Rahimi, P. Dong, and C. Jung, “Global NDVI-LST correlation: Temporal and spatial patterns from 2000 to 2024,” *Environments*, vol. 12, no. 2, p. 67, 2025.
[17] M. O. Sarif, B. Rimal, and N. E. Stork, “Assessment of changes in land use/land cover and land surface temperatures and their impact on surface urban heat island phenomena in the kathmandu valley (1988–2018),” *ISPRS International Journal of Geo-Information*, vol. 9, no. 12, p. 726, 2020.